AIAA JOURNAL
Vol. 49, No. 6, June 2011

Feedforward Adaptive-Optic Correction of Aero-Optical Aberrations Caused by a Two-Dimensional Heated Jet

Daniel A. Duffin* and Eric J. Jumper†
University of Notre Dame, Notre Dame, Indiana 46556

DOI: 10.2514/1.J050904

A feedforward adaptive-optic correction was made on a known, repeatable aero-optical aberration caused by a two-dimensional heated jet. Since the bandwidth requirements for traditional closed-loop adaptive-optic correction are significantly higher than current technology limitations, an unconventional feedforward adaptive-optic correction scheme was experimentally tested to determine the feasibility of adaptive-optic corrections for aero-optical disturbances in general. The feedforward adaptive-optic approach was successful in correcting aero-optical disturbances at a frequency of 240 Hz, as evidenced through Shack–Hartmann wave front sensor measurements. The feedforward correction scheme exceeded simulated performance predictions when it was able to boost the time-averaged Strehl ratio from 0.64 without correction to 0.88 with correction.

Nomenclature

D	=	jet exit nozzle width
f	=	frequency
n	=	index of refraction
n'	=	index-of-refraction fluctuation
$\mathrm{OPD}_{\mathrm{rms}}$	=	root-mean-square optical path difference
s	=	beam propagation path
t	=	time
U_c	=	convection velocity
x, X	=	streamwise (flow) direction
y, Y	=	cross-stream (propagation) direction
z, Z	=	spanwise direction
θ	=	beam deflection angle
λ	=	wavelength
τ	=	temporal latency
φ	=	phase error
φ_{rms}	=	root-mean-square phase error
ω	=	angular frequency

Introduction

AERO-OPTICS is the study of flowfield effects on optical beams that are transmitted through the flowfield. When an optical beam with an otherwise collimated, planar wave front is transmitted through a turbulent index-of-refraction-variant flowfield, the optical beam becomes distorted due to the index-of-refraction variations throughout the flowfield. These index-of-refraction variations in the flow imprint a phase error, or aberration, upon the initially planar optical wave front. The aberrations to the wave front are not static; rather, the emerging wave front is imprinted with time-varying aberrations, as seen in Fig. 1.

These dynamic aberrations degrade the ability for the beam to be focused in the far field, and they can reduce the far-field intensity by more than 95% [1]. It has long been known that if the conjugate waveform of the aberration is placed on the optical beam before its transmission through the aberrating flow, the beam will emerge with a planar wave front. This is the basis for adaptive-optic correction [2]. One can use a deformable mirror (DM), or some other device, to imprint this conjugate waveform onto the optical beam and then propagate the beam through the flowfield. The emerging beam will then focus in the far field, and its far-field intensity will effectively peak back up to 100% of its diffraction-limited intensity. The adaptive-optic correction scheme is illustrated in Fig. 2, along with far-field intensity patterns of the aberrated and corrected cases.

Aberrated wave fronts are commonly described by either their optical path length (OPL) or their optical path difference (OPD). OPL is defined as the integral of the index of refraction along the path that the optical beam travels:

$$\mathrm{OPL}\,(x, z, t) = \int_{s_1}^{s_2} n(x, y, z, t)\,\mathrm{d}s \approx \int_{y_1}^{y_2} n(x, y, z, t)\,\mathrm{d}y \qquad (1)$$

where s_1 and s_2 are the entrance and exit positions, respectively, along the path the beam takes through the flowfield [3]. This integration is not strictly performed in the y direction, because the optical beam takes a curved three-dimensional path through the flowfield, as illustrated in Fig. 3. For most cases though, the aberrations are small enough to allow integration in the y direction alone, without introducing much error in the OPL; this is common practice.

The OPD is the spatial-mean-removed OPL:

$$\mathrm{OPD}\,(x, z, t) = \mathrm{OPL}(x, z, t) - \overline{\mathrm{OPL}}(t) \qquad (2)$$

The OPD provides all of the information needed to construct conjugate waveforms for use with an adaptive-optics system. However, there are two major problems associated with making traditional closed-loop adaptive-optic corrections for aero-optics. First, the speed at which the OPD of the aberrated wave fronts must be captured is much higher than the capability of most state-of-the-art wave front sensing devices. Second, once the conjugate correction is computed from the measured OPD, it must be sent to the adaptive-optics system fast enough that the correction applied at a specific time is still valid for the flowfield at that time. This second issue deals mostly with computer-induced time-delay issues and problems currently associated with real-time processing. Work performed at the University of Notre Dame during the Summer of 2004 demonstrated that high-speed wave front measurements (100 + kHz) can be made through the use of postprocessing [4,5]. This still does not address the second problem associated with traditional adaptive-optic corrections: the real-time application of these conjugate

Presented as Paper 2005-4776 at the 36th AIAA Plasmadynamics and Lasers Conference, Toronto, 6–9 June 2005; received 3 September 2010; revision received 20 December 2010; accepted for publication 27 December 2010.

*Graduate Research Assistant/National Defense Science and Engineering Graduate Fellow, Center for Flow Physics and Control, Department of Aerospace and Mechanical Engineering. Member AIAA.

†Professor, Center for Flow Physics and Control, Department of Aerospace and Mechanical Engineering. Fellow AIAA.

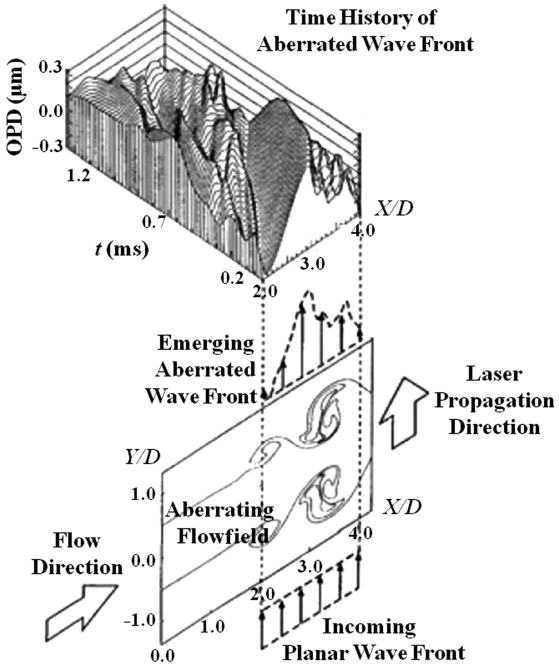

Fig. 1 Time history of aberrated wave fronts [1,6].

corrections. This second problem may take many years to ultimately solve; however, the work described in this paper explored the feasibility of adaptive-optic corrections by incorporating flow control into a feedforward adaptive-optics system in order to achieve the bandwidths required to make the corrections.

Feedforward control differs from feedback control by the manner in which the error signal (wave front error in this case) is controlled. A closed-loop feedback controller measures the actual error output from the system (plant) directly and sends commands back to the plant to compensate for the error, whereas a feedforward controller measures the input disturbance to the system and sends compensating commands forward to the plant without measuring the actual system output error in real time. Feedforward control can be much faster than feedback control, as it does not require the delay time involved with measuring the actual system output error; however, feedforward control is best suited to well-understood systems (i.e., processes that follow fundamental physical laws). Turbulent fluid flow is not typically thought of as a well-understood physical process, but as will be seen, with the inclusion of flow control, the aero-optic flowfield of interest was turned from a random process into a well-understood highly periodic process suited to feedforward control. Basically, the feedforward adaptive-optics approach discussed here involved using postprocessed wave front

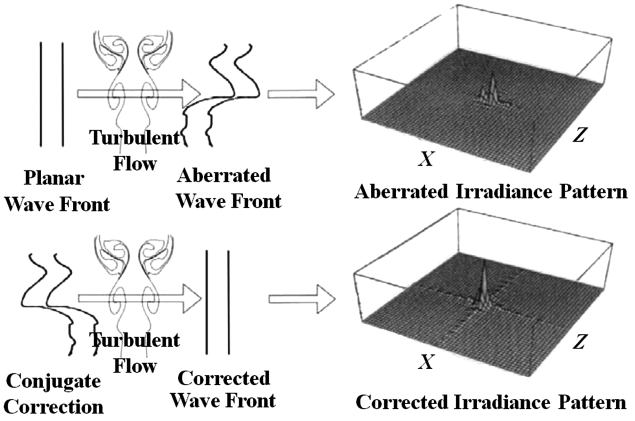

Fig. 2 Adaptive-optic correction theory and corresponding far-field intensity patterns.

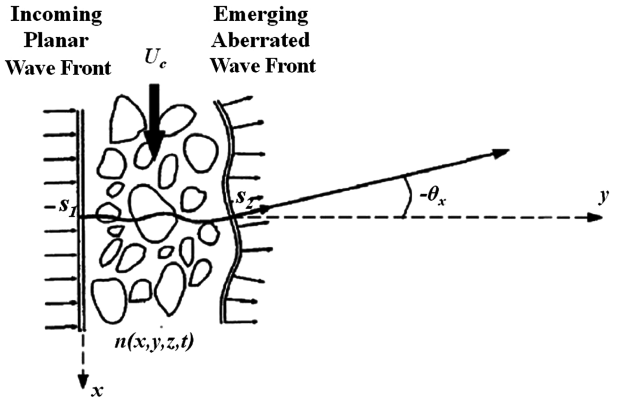

Fig. 3 Optical ray path through a convecting index-of-refraction-variant flowfield.

measurements in order to characterize the flowfield a priori, ultimately driving a DM with compensation commands derived from the input disturbance (flow control) signal in order to correct for the wave front aberrations caused by the laser beam propagating through the flowfield.

Experimental Setup

Two-Dimensional Heated-Jet Facility

The aero-optic flowfield used for this study was a two-dimensional heated jet. The heated-jet facility is shown schematically in Fig. 4. A plenum chamber was pressurized above atmospheric pressure by a blower. After passing through filters and a slight contraction, the pressurized air entered a rectangular duct and passed over a series of heaters located approximately 1 m downstream. The heated air then flowed through a 90 deg finned bend located 1 m from the heater section. The air then moved vertically through filters and flow straighteners, as shown in Fig. 4. The heated air passed through a 16:1 two-dimensional nozzle with an exit plane nozzle width D of 1.27 cm. The heated jet left the nozzle with a core velocity of 7 m/s. The detailed fluid mechanic measurements for this jet can be found in [6].

Figure 5 shows a schematic of the exit plane of the jet nozzle. The left side of the figure shows the view normal to the jet (the aero-optic view), its span dimension (30 cm), and the end plates aligned in the streamwise x direction to help reduce three-dimensional effects that

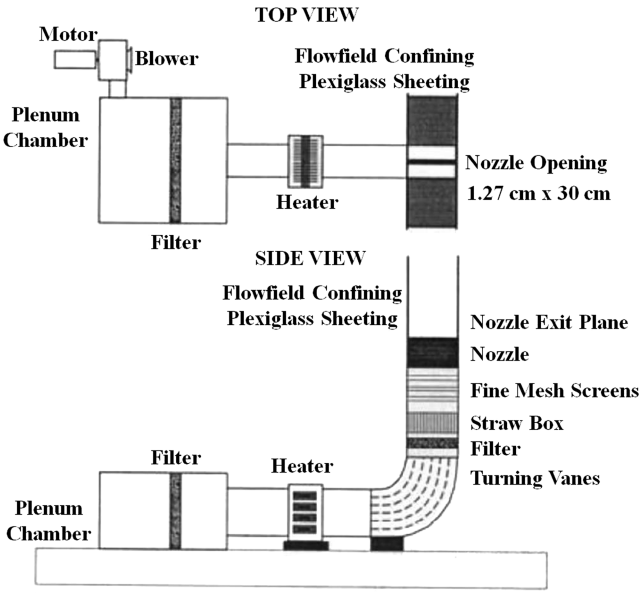

Fig. 4 Two-dimensional heated-jet facility [6].

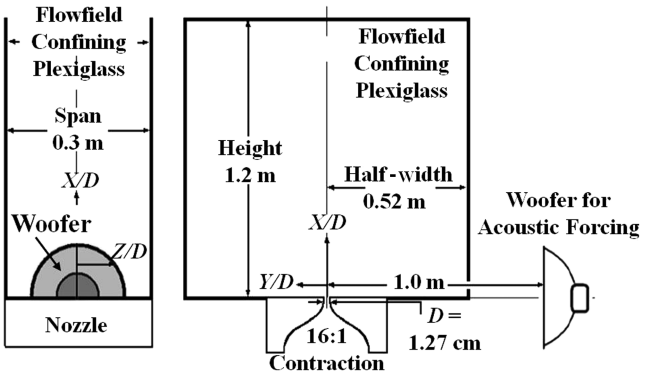

Fig. 5 Heated-jet exit plane schematic.

would otherwise be present if the jet were uncontained. The right side of the figure shows the view along the z direction of the jet, and it contains a number of important details. First, the jet exit plane formed a solid floor that extended for 0.52 m in each direction from the nozzle gap, which allowed entrainment air to be brought in normal to the jet. Second, the location and orientation of a speaker used to force the flow is shown; the speaker was located in the exit plane 1 m from the centerline of the nozzle.

Jet Response to Acoustic Forcing

The details of the jet response to flow control via acoustic forcing can be found in [7]. It is sufficient here to briefly describe the jet characteristics as they pertain to this current work. The acoustic forcing was provided by a Pyramid PWFX107 600 W 10 in. woofer, located as shown in Fig. 5. The speaker was driven by a Crown CE2000 power amplifier with an input provided by an Agilent model 33120A function/arbitrary waveform generator. In the present case, the jet was forced with a 240 Hz sine waveform.

Jet response to the 240 Hz forcing was to regularize the most-unstable Kelvin–Helmholtz instability in the jet's two bound shear layers (one shear layer develops off of each edge of the nozzle lip and always stays attached to that edge). Depending on the amplitude of the acoustic signal, the 240 Hz vortex roll up could be adjusted closer to or further away from the nozzle exit plane. The forcing also regularized the first vortex pairing event, resulting in the formation of 120 Hz subharmonic larger-coherence-length flow structures; however, this regularization is slightly less robust than the first roll up. To provide the best overall regularization for this experiment, the amplitude of the acoustic forcing signal caused the 240 Hz roll up to occur somewhat closer to the exit plane than documented in earlier

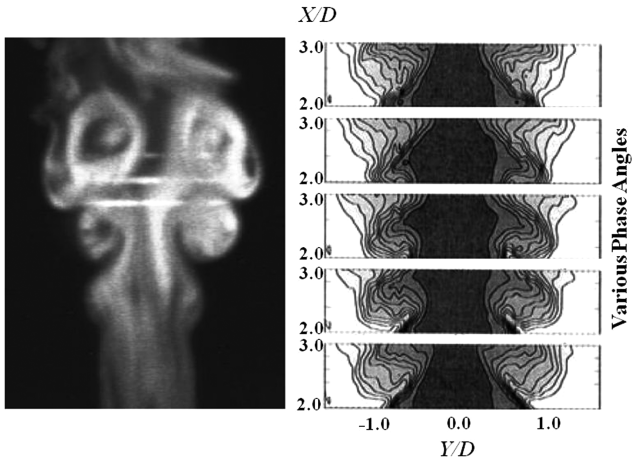

Fig. 6 Smoke visualization of the two-dimensional heated jet (left) and phase-averaged temperature profiles of acoustically forced jet (right) [8].

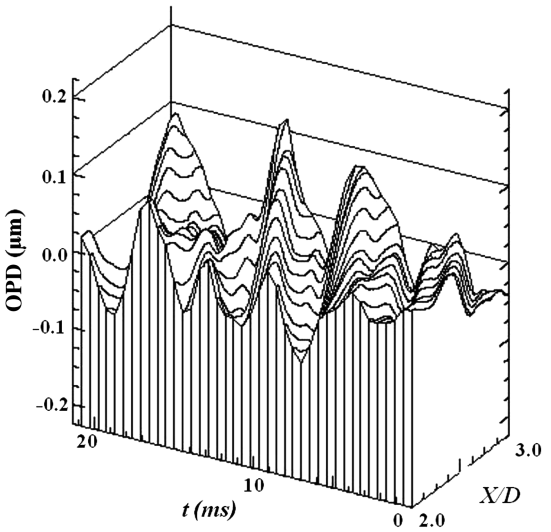

Fig. 7 Time series of experimentally measured OPDs from propagation through the two-dimensional heated jet without acoustic forcing [9].

forcing studies, which concentrated primarily on the initial vortex roll-up event [8,9]. The results from the earlier forcing studies are qualitatively similar to results with the current configuration. Results from these earlier tests are shown in Figs. 6–8 in order to illustrate certain points about the acoustically forced heated-jet flow physics. A smoke visualization and a phase-locked averaged temperature field collected for the acoustically forced heated jet are shown in Fig. 6. Figures 7 and 8 show the effect that the acoustic forcing had on the jet OPD pattern. Figure 7 is the heated-jet OPD pattern without acoustic forcing. One should note that the OPD peaks are quite random, and while there is a certain temporal frequency to this pattern, there are also large deviations about this frequency. Figure 8 shows that acoustic forcing regularizes both the amplitude of the OPD as well as the temporal frequency of the pattern. It is this predictable, repeatable type of OPD pattern that makes a feedforward adaptive-optic experiment feasible.

Phase-Locked Averaged Wave Front Measurements

The periodic nature of the acoustically forced heated jet gives one the ability to perform phase-locked averaging on the jet wave fronts

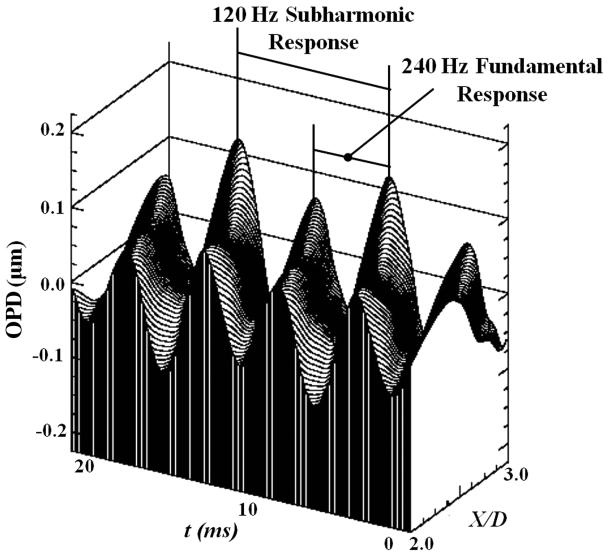

Fig. 8 Time series of experimentally measured OPDs from propagation through the two-dimensional heated jet with acoustic forcing [13].

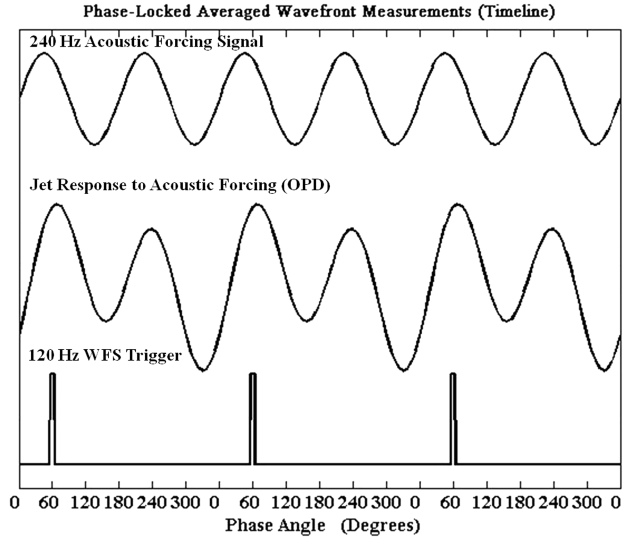

Fig. 9 Phase-locked average wave front measurement technique (WFS denotes wave front sensor).

in order to obtain a representative set of wave fronts that completely describes a single full cycle of the jet response. Although the jet was forced at 240 Hz, Fig. 8 shows that there was a 120 Hz subharmonic oscillation present along with the 240 Hz fundamental aberration in the OPD measurements. Thus, in order to obtain a representative cycle of the jet response, which captured all the physics of the aberrated flow, the phase-locked averaging was performed on this 120 Hz subharmonic cycle instead of the 240 Hz fundamental cycle. The phase-locked averaging was performed using a Wavefront Sciences CLAS-2D wave front sensor. The CLAS-2D wave front sensor is a two-dimensional Shack–Hartmann-type wave front sensor, as described in [4,10]. The wave front sensor was triggered to capture wave fronts at specific phase angles over the 120 Hz subharmonic repeat cycle, as shown in Fig. 9.

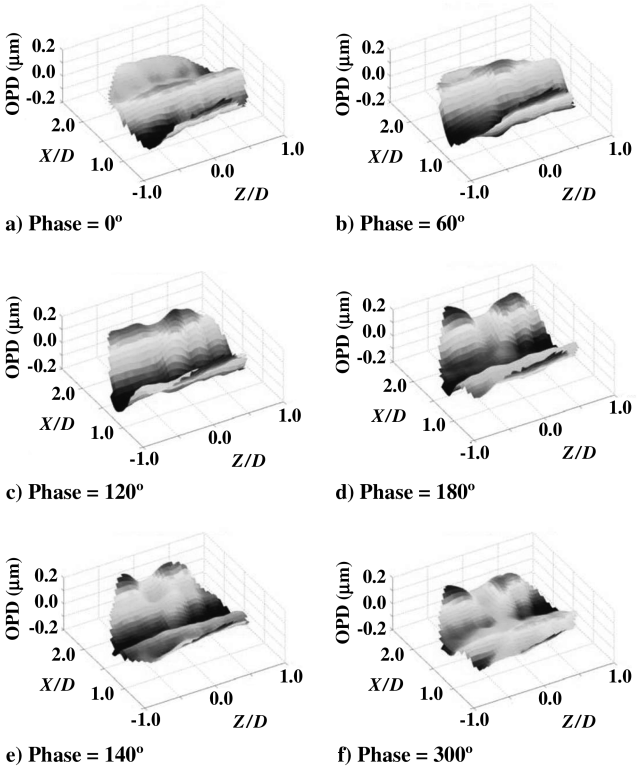

Fig. 10 Phase-locked averaged wave fronts obtained with Wavefront Sciences CLAS-2D wave front sensor at various phase angles ($0.5 < X/D < 2.5$; $-1.0 < Z/D < 1.0$; and OPD scale in micrometers).

Thirty-six phase angles over the 120 Hz subharmonic cycle were used with a separation between angles of 10 deg in order to cover the full 360 deg cycle. At each phase angle, 200 wave front measurements were taken with the triggered CLAS-2D wave front sensor and averaged together to obtain the representative wave front for that phase angle. Figure 10 shows some of the phase-locked averaged wave fronts obtained from this analysis. Since the vortex structures comprise low index-of-refraction cores, the consecutive roll up and convection of vortices in the flow results in the peak-and-valley wave structure that convects downstream with increasing phase angle, as seen in Fig. 10. Also, since the flowfield is uniform in the span direction, one should expect to see highly one-dimensional wave front error patterns. Finally, due to the influence of the 120 Hz subharmonic, there should be discernible variation in the shape of the wave fronts from a certain phase during the fundamental 240 Hz period to the subsequent 240 Hz period (i.e., phase $= 0°$ as compared with phase $= 180°$).

Notre Dame Adaptive-Optics System

During the summer of 2003, the University of Notre Dame accepted delivery of a relatively low-bandwidth adaptive-optics system designed and constructed by Xinetics, Inc., in conjunction with Boeing–SVS. Since that time, the adaptive-optics system has been used to make closed-loop adaptive-optic corrections for aberrations of $\sim$10 Hz (i.e., optical distortions caused by helium rising through air and optical distortions caused by the flame of a small candle in air).

The DM that is a part of this adaptive-optics system has a diameter of 49 mm and is driven by 37 piezoelectric actuators attached to the rear face of the mirror. The actuators have a stroke of ± 4 μm, which is more than enough to correct for the optical aberrations seen in the heated jet, which are on the order of ± 0.1 μm. A schematic of the DM is shown in Fig. 11. The DM can be driven to about 5 kHz before significant magnitude and phase changes in the mirror response, which was more than sufficient for the feedforward testing described here. A Bode response plot of one of the mirror's actuators is shown in Fig. 12. This feedforward test decoupled the DM from its traditional adaptive-optics system and drove it, in a feedforward sense, with analog signals derived from the phase-locked averaged OPD measurements shown in Fig. 10. To perform this task, a 37-channel digital-to-analog system was assembled from five National Instruments analog-output cards, as described next. These signal generators were driven with digital time histories obtained from the postprocessed phase-locked averaged OPD results, producing the necessary conjugate corrections on the DM.

The wave front sensor that is incorporated into this adaptive-optics system is a Shack–Hartmann sensor that can collect wave fronts at 1 kHz. This wave front sensor was used as a scoring sensor to collect

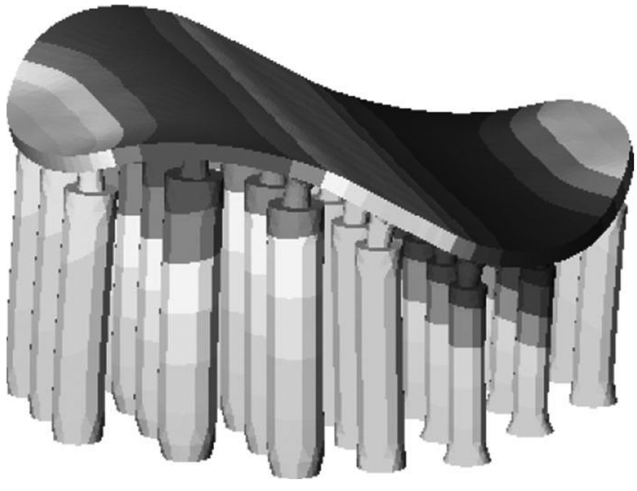

Fig. 11 Schematic of University of Notre Dame's Xinetics DM.

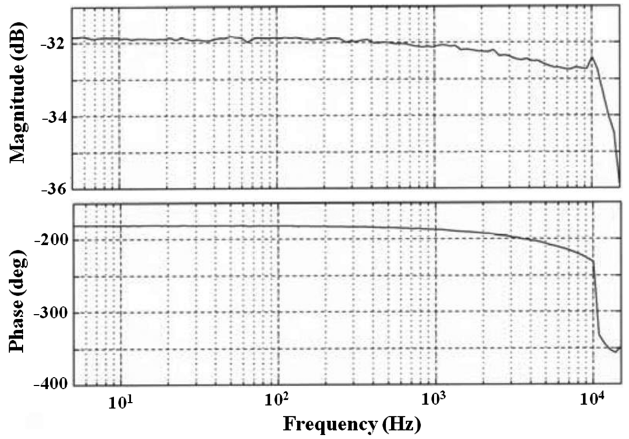

Fig. 12 Response of single piezoelectric actuator on University of Notre Dame's Xinetics DM.

the resulting corrected wave fronts from the feedforward adaptive-optic experiments. These wave front data were used to determine how well the adaptive-optic experiments were able to correct for the heated-jet aberrations. From these wave fronts, far-field patterns were computed and time histories of Strehl ratios were obtained [6].

Optical Train Schematic

A planar, collimated 2.54-cm-diam laser beam was propagated through the heated jet perpendicular to the jet (in the *y* direction, as seen in Fig. 5). The index-of-refraction variations in the acoustically forced heated jet imprinted periodic aberrations onto the laser beam, as discussed previously. This aberrated beam was then steered into the adaptive-optics system. The beam was routed through the adaptive-optics system, as shown in Fig. 13.

In Fig. 13, BS means beam splitter, T/T means tip/tilt, WFS means wave front sensor, and all of the other optics are noted on the schematic. The lighter beam signifies that the beam wave front is aberrated, while the darker beam wave front has been corrected. As one can see from the schematic the wave front sensor was used to record the wave fronts of the adaptive-optically corrected beam for scoring purposes.

Thirty-Seven-Channel Analog-Output Driver System

To drive the Xinetics DM, a 37-channel analog-output system was assembled. The system consisted of five National Instruments NI PXI-6733 eight-channel 16-bit analog-output boards. These boards have an update rate of one megasample per second, which is sufficient to update each channel analog signal at upward of 40 kHz.

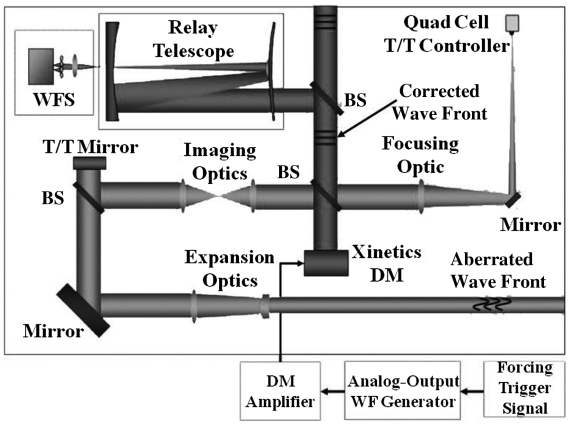

Fig. 13 Schematic of optical train and electronics (WF denotes wave front).

For this experiment, the analog signals were updated 72 times during each 120 Hz subharmonic repeat cycle. To keep all of the analog-output cards synchronized, their onboard timing oscillators were controlled by a National Instruments NI PXI-6652 timing and synchronization module, which has a high-resolution clock generation at 10 MHz with a 711 nHz resolution.

The wave front data collected by the Wavefront Sciences CLAS-2D wave front sensor were conjugated, and these conjugate corrections were turned into the voltage information needed to drive the DM by a National Instruments Analog Waveform Editor software package. These voltage data were then stored in the onboard first in/first out (FIFO) memory on the NI PXI-6733 cards. The entire system was triggered to the acoustic forcing signal. When the analog-output system received a trigger, it automatically read out the data stored in the FIFO memory to the 37 analog-output channels at the update rate discussed previously. The National Instruments system free ran at the mentioned update rate until a stop signal was sent to the system. The reference clock imbedded in the PXI-6652 timing module kept the analog-output synchronized to the forcing signal. Initial testing with the system has shown that the timing module has been able to keep the analog-output signals synchronized to the forcing signal for over 1 h.

Simulation Benchmark

A benchmark for this adaptive-optic test was obtained by performing the experiment in an offline computer simulation [5]. A high-bandwidth wave front sensor was used to collect wave fronts from the two-dimensional heated jet at 125 kHz. These wave fronts were phase averaged, and the phase-averaged OPDs were turned into their conjugate corrections. These conjugate corrections (as a function of phase angle) were then added (at the appropriate phase) to the time history of instantaneous wave fronts collected by the sensor. This resulted in a time history of simulated corrected wave fronts. From the time series of corrected wave fronts, Fourier optics were used to determine the far-field intensity patterns of these simulated corrected wave fronts. The Strehl ratios (the ratio of on axis intensity to diffraction-limited on axis intensity) for these corrected wave fronts were extracted from the far-field intensity patterns. Figure 14 shows the results from this analysis. The dotted line represents the case when no adaptive-optic correction is applied. Deep drops in the Strehl ratio are apparent when vortical structures pass across the beam aperture, causing the Strehl ratio to drop to around 0.4. The average Strehl ratio was about 0.7 for the case without correction, meaning an average loss of 30% of the intensity on the target. However, when the adaptive-optic correction scheme was applied, the Strehl ratio is dramatically improved, shown by the solid line. The

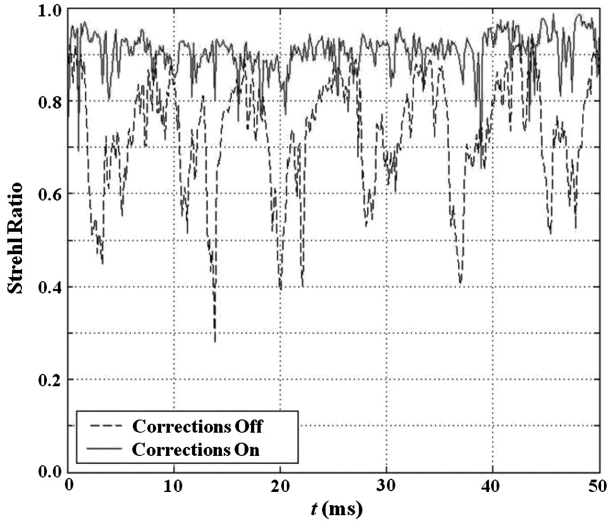

Fig. 14 Time history of Strehl ratio with and without simulated adaptive-optic correction [5].

average Strehl ratio was about 0.88 for the case with adaptive-optic correction.

This simulation benchmark set the goal for the laboratory experiment. In this computer simulation, the phase-locked average conjugate corrections were exactly added to the free-running wave fronts from the acoustically forced heated jet; thus, the residual Strehl ratio degradation for the corrections-on scenario represents the cycle-to-cycle variation in the wave fronts. A second limitation imposed on the experiment was the fact that, in the test series reported here, the conjugate correction used was two-dimensional; that is, the mirror surface was uniform in the z (spanwise) direction (Fig. 10 shows that this is only approximately true). In the simulation, the full three-dimensional phase-locked averaged conjugate correction was applied.

Experimental Results

During this experiment, the Xinetics wave front sensor captured wave fronts at 1 kHz, which provided approximately eight wave front realizations during the jet's 120 Hz subharmonic repeat cycle. Two major test cases were evaluated: one with no adaptive-optic correction (DM off) and the other with feedforward adaptive-optic correction (DM on). Results from both cases will be compared directly in order to gauge the success of the experiment. The wave front data were also used to compute far-field patterns and Strehl ratios for further comparison.

Wave Front Results

Figure 15 shows wave front surface plots for the two experimental cases. These results show four wave front realizations during one 120 Hz subharmonic cycle of aberration. These results are typical and representative of the entire data set.

In Figs. 15b and 15c, one can clearly see a large-scale aberration due to a vortical structure passing through the optical beam. When the DM is run to correct the optical aberrations, one can see that the large-scale aberrations are no longer seen on the beam wave fronts (Figs. 15e–15h). These last four figures show that the adaptive-optic correction effectively removes all of the large-scale aberrations on the beam. The corrected beam still has some small-scale aberrations present. These small-scale aberrations are more random in the heated

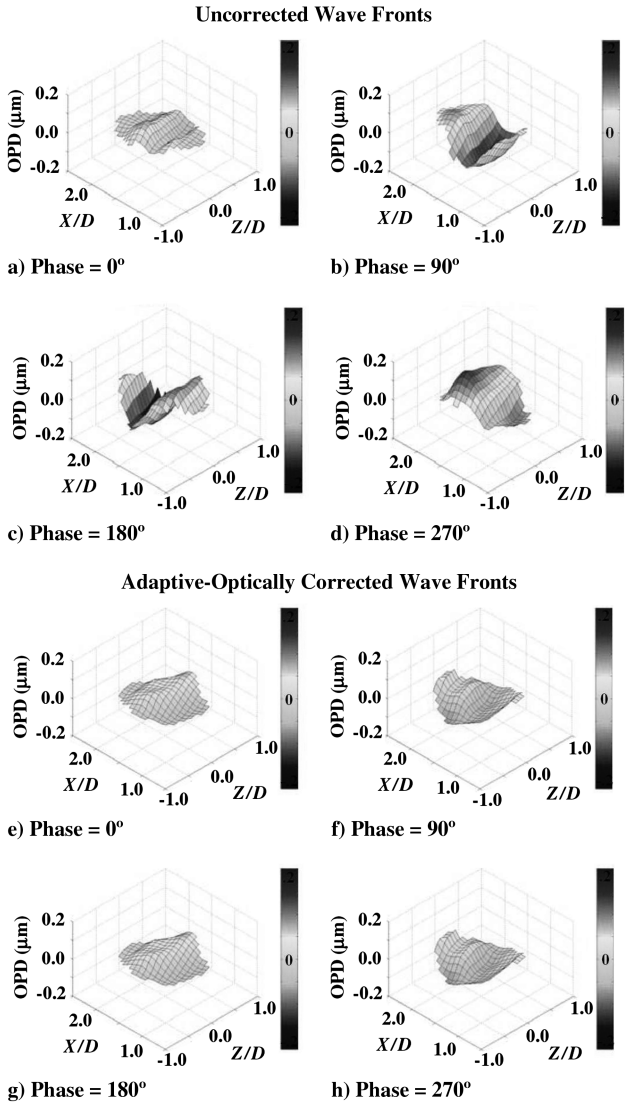

Fig. 15 Typical instantaneous wave fronts (three-dimensional view) obtained with the Xinetics wave front sensor at various phase angles: a–d) uncorrected wave fronts and e–h) adaptive-optically corrected wave fronts ($0.5 < X/D < 2.5$; $-1.0 < Z/D < 1.0$; and OPD scale in micrometers).

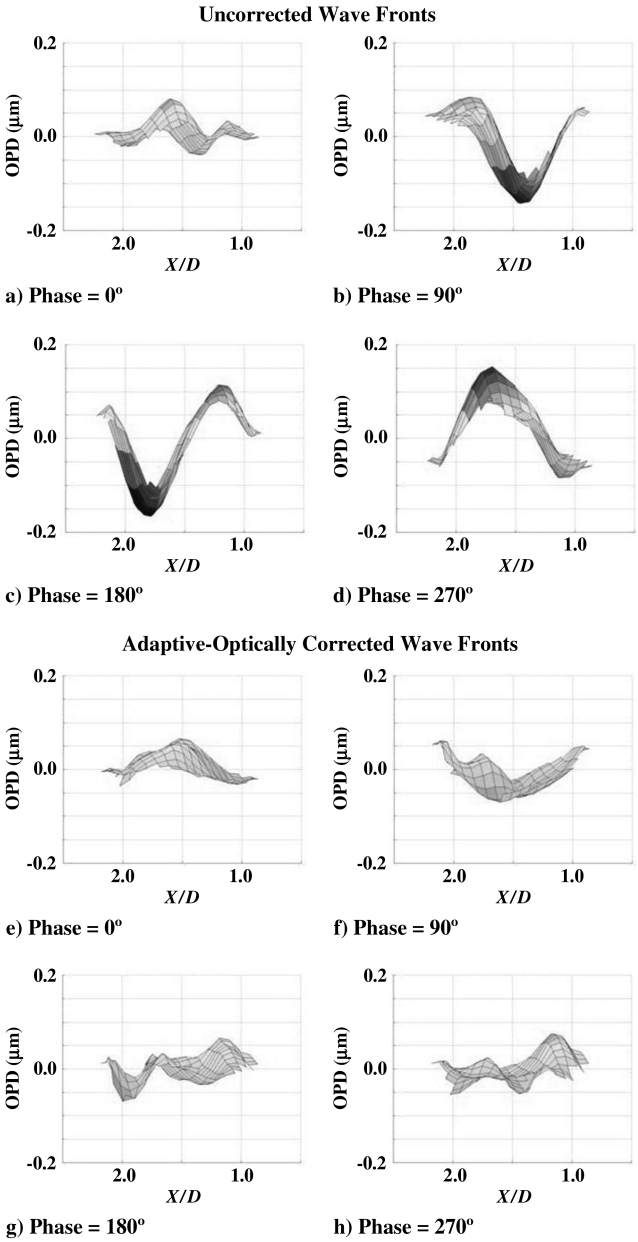

Fig. 16 Typical instantaneous wave fronts (side view) obtained with the Xinetics wave front sensor at various phase angles: a–d) uncorrected wave fronts and e–h) adaptive-optically corrected wave fronts ($0.5 < X/D < 2.5$; $-1.0 < Z/D < 1.0$; and OPD scale in micrometers).

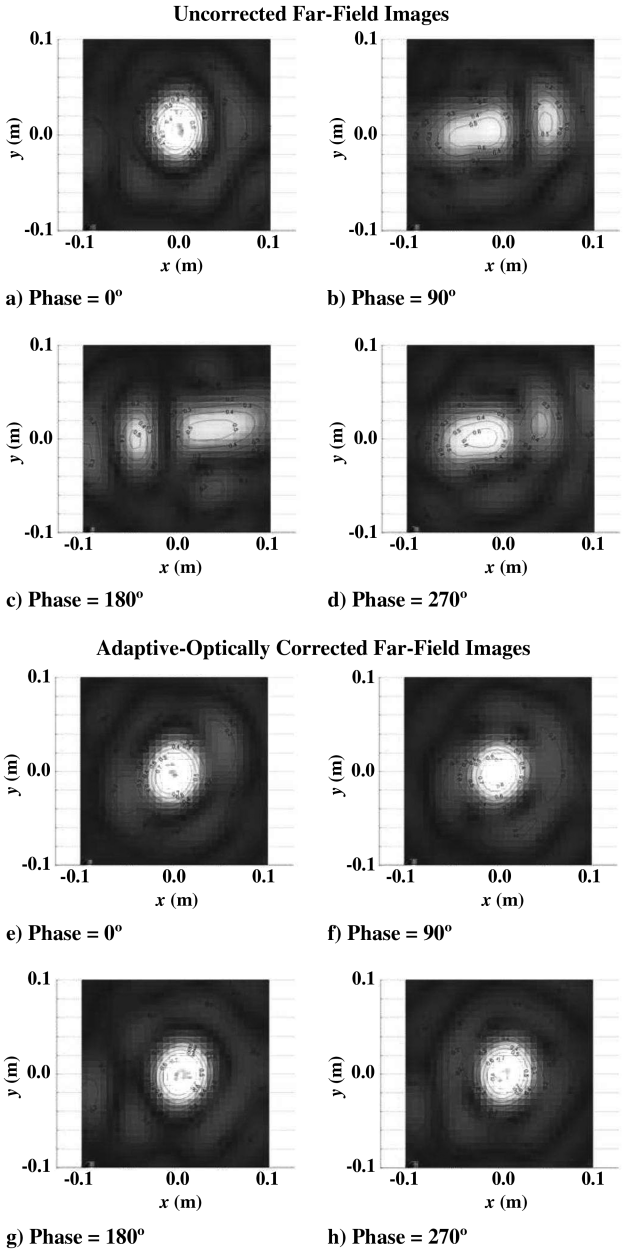

Fig. 17 Typical instantaneous far-field images obtained with Fourier optics code at various phase angles: a–d) uncorrected far-field images and e–h) adaptive-optically corrected far-field images.

jet, and not the organized large-scale vortical structures that the phase-locked averaged wave front results show. There is also some three-dimensional residual error on the corrected beam. The correction applied by the mirror was two-dimensional uniform in the z (spanwise) direction; however, Fig. 10 clearly shows the presence of small three-dimensional variations in the acoustically forced heated jet that now shows up as a residual error in the corrected wave fronts due to the purely two-dimensional adaptive-optic correction used in the experiment.

It is hard to determine the peak-to-peak OPD by looking at the plots in Fig. 15. Figure 16 shows the same wave front realizations, except shown on end so that the amplitudes of the wave fronts can be clearly seen.

Figure 16 shows more clearly just how much the amplitude of the wave front error was reduced by using the feedforward adaptive-optic correction scheme. The average peak-to-peak OPD for the uncorrected case is 0.245 μm, and that is reduced to an average peak-to-peak value of 0.148 μm for the adaptive-optically corrected case. These wave front plots are clear proof that the feedforward

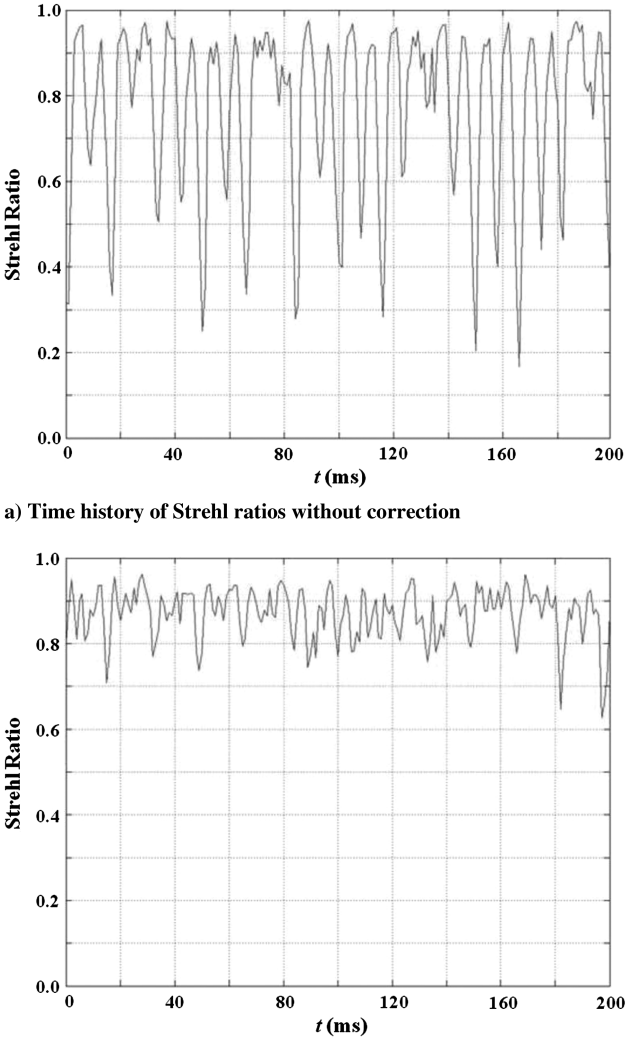

a) Time history of Strehl ratios without correction

b) Time history of Strehl ratios with correction

Fig. 18 Time history of Strehl ratio a) without and b) with adaptive-optic correction.

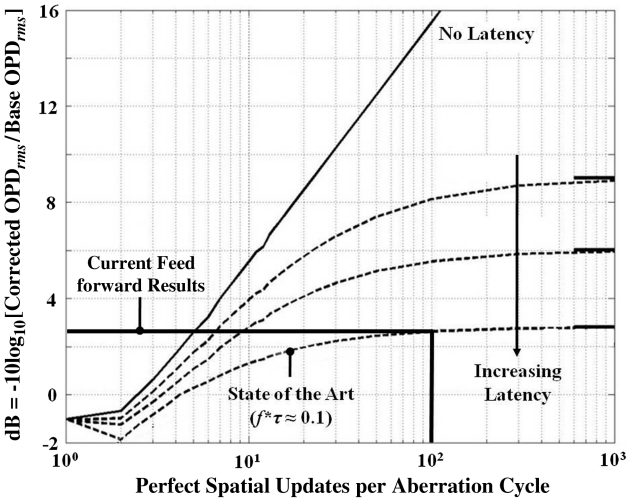

Fig. 19 Bandwidth requirements for traditional closed-loop adaptive-optic systems.

adaptive-optic experiment was a success. For the entire experiment, the root-mean-square value of OPD for the case with no correction was 0.0616 μm, and this value was reduced to 0.0359 μm when the correction scheme was used: an improvement of 42%.

Far-Field Images and Strehl Ratio Plots

Fourier optics were used to calculate far-field irradiance patterns from the wave front information in Figs. 15 and 16. One can see in Figs. 17b and 17c that, as the vortical structure passes by, the beam essentially breaks apart in the far field, losing all ability to focus on a single point. This degradation in the far-field pattern results in an intensity on target of only 20–30% of a diffraction-limited beam intensity on target. When the adaptive-optic correction scheme is implemented, the beam never breaks down in the far field; rather, it remains essentially focused at the target. While the adaptive-optic correction is used, the beam intensity never drops below 64% of its diffraction-limited intensity.

A time history of the Strehl ratio (as in Fig. 14) would give one the ability to see just how well the feedforward adaptive-optic correction scheme performed. Figure 18 shows two time histories of the Strehl ratio: one for the uncorrected case and one for the adaptive-optically corrected case. Comparing Fig. 18 to Fig. 14, one can see that the adaptive-optic experiment performed as well as the simulation benchmark and, in some cases, exceeded the performance predicted by the simulation. The average Strehl ratio for the case with no correction was 0.64, while the average Strehl ratio for the case with adaptive-optic correction was 0.88. This is an improvement of 38% in the Strehl ratio, which exceeds the improvement of 25% seen in the simulation.

Conclusions

The feasibility of the flow-control-based feedforward adaptive-optic approach has been demonstrated, and the results from this demonstration have exceeded a simulated best-case scenario. The experimental results exceeding the simulated results is somewhat surprising for two reasons. First, the simulation made use of a full three-dimensional correction as opposed to the two-dimensional correction used in the experiment. Second, the simulation imposed the exact phase-locked correction, whereas the experiment relied on the mirror's slightly incorrect realization of the electronically imposed voltage pattern. One possible explanation for this discrepancy is that the wave front sensor used in the simulation had only a 4×4 lenslet array and could have missed some of the structure that the 33×44 lenslet array, which the experimental wave front was based upon, was able to resolve. Thus, the experimental wave front, although two-dimensional, was able to resolve, and thus remove, more of the aberrating structure than the simulation was capable of removing.

This feedforward approach has also been scaled up and applied to a Mach 0.8 free shear layer facility that mimics the aero-optic aberrations expected at flight conditions [11,12]. In the higher-Mach experiment, the frequency of the disturbances increased fourfold and the aberration magnitude increased approximately fivefold; yet, this same feedforward adaptive-optic correction scheme was able to improve the Strehl performance in that scenario as well. The key to the success of this feedforward approach lies in the ability to regulate the flowfield of interest. It does not seem logical that a turbulent flow could be organized, but the physical processes behind these shear layer flows dictate a specific underlying vortical aberration pattern. Turbulence is not always random, and flow control really only assists the natural vortex shedding process. This correction approach could prove important to many of the current flight-based optical systems. The use of flow control to robustly regulate a flowfield could make it easy to predict and correct for aero-optical aberrations based on a handful of simple inputs: altitude, speed, and optical line of sight. This approach could also be used in conjunction with a conventional closed-loop system to assist in the correction of the high-speed aberrations that lie outside of the bandwidth of the closed-loop system.

The historic significance of this experiment can be appreciated if one compares the success of this experiment and its feedforward approach to what would be needed to make traditional adaptive-optic corrections. Figure 19 shows the results of a simple adaptive-optic simulation that was constructed in order to understand how timing issues affect the correctability of a beam using a conventional adaptive-optics scheme [12]. This simulation shows how much relative correction (corrected $\mathrm{OPD}_{\mathrm{rms}}$/uncorrected $\mathrm{OPD}_{\mathrm{rms}}$) a specific adaptive-optic system configuration (update rate and latency) would give. The feedforward experiment discussed previously realized a relative correction of 2.34 dB. For a state-of-the-art traditional adaptive-optics system with a nominal amount of latency, Fig. 19 suggests that an update rate of 24 + kHz would be needed in order to realize the amount of adaptive-optic correction seen in this feedforward experiment. These system configuration requirements are far beyond the limitations of even modern adaptive-optics systems.

When a wave front aberration process is well understood, or can be made to be well understood, one no longer needs to rely on conventional closed-loop adaptive-optic control; rather, one can incorporate a priori information about the processes into a feedforward adaptive-optic correction scheme in order to make timely and accurate wave front corrections. By using this unconventional feedforward approach, adaptive-optic corrections have been made that have resulted in a Strehl ratio recovery of 0.88. This experiment has produced results expected from a 24 + kHz traditional adaptive-optics system, while today's state-of-the-art traditional adaptive-optics systems hover around 1 kHz.

Acknowledgments

These efforts were sponsored by the U.S. Air Force Office of Scientific Research, U.S. Air Force Material Command, under grant number F49620-03-1-0019. The authors thank the American Society of Engineering Education for their financial support through the National Defense Science and Engineering Graduate Fellowship.

References

[1] Jumper, E. J., and Fitzgerald, E. J., "Recent Advances in Aero-Optics," *Progress in Aerospace Sciences*, Vol. 37, No. 3, 2001, pp. 299–339. doi:10.1016/S0376-0421(01)00008-2

[2] Tyson, R. K., *Principles of Adaptive Optics*, 2nd ed., Academic Press, Chestnut Hill, MA, 1991, pp. 53–100.

[3] Jumper, E. J., and Hugo, R. J., "Quantification of Aero-Optical Phase Distortion Using the Small-Aperture Beam Technique," *AIAA Journal*, Vol. 33, No. 11, 1995, pp. 2151–2157. doi:10.2514/3.12960

[4] Duffin, D. A., Gordeyev, S., and Jumper, E. J., "Comparison of Wavefront Measurement Techniques on a Two Dimensional Heated Jet," AIAA Paper 2004-2446, June 2004.

[5] Gordeyev, S., Duffin, D. A., and Jumper, E. J., "Aero-Optical Measurements Using Malley Probe and High Bandwidth 2-D Wavefront Sensors," International Conference on Advanced Optical Diagnostics in Fluids, Solids and Combustion, VSJ-SPIE04, Tokyo, Paper V0020, Dec. 2004.

[6] Hugo, R. J., "Quantifying the Spatio-Temporal Effects of Optically-Active Turbulent Flowfields on a Coherent Optical Wave," Ph.D. Dissertation, Aerospace and Mechanical Engineering Dept., Univ. of Notre Dame, Notre Dame, IN, 1995.

[7] Duffin, D. A., Gordeyev, S., and Jumper, E. J., "Visualizing Index-of-Refraction Variations in Optically Active Flow Fields," 11th International Symposium of Flow Visualization Conference, ISV11, Paper 075, Edinburgh, 2004.

[8] Hugo, R. J., and Jumper, E. J., "Applicability of the Aero-Optic Linking Equation to a Highly Coherent, Transitional Shear Layer," *Applied Optics*, Vol. 39, No. 24, Aug. 2000, pp. 4392–4401. doi:10.1364/AO.39.004392

[9] Hugo, R. J., and Jumper, E. J., "Experimental Measurement of a Time-Varying Optical Path Difference by the Small-Aperture Beam Technique," *Applied Optics*, Vol. 35, No. 22, Aug. 1996, p. 4436. doi:10.1364/AO.35.004436

[10] Geary, J. M., "Introduction to Wavefront Sensors," *Tutorial Texts in Optical Engineering*, Vol. TT18, Soc. of Photo-Optical Instrumentation Engineers Optical Engineering Press, Bellingham, WA, 1995, pp. 89–

104.
[11] Rennie, R. M., Duffin, D. A., and Jumper, E. J., "Characterization and Aero-Optic Correction of a Forced Two-Dimensional Weakly Compressible Shear Layer," *AIAA Journal*, Vol. 46, No. 11, 2008, pp. 2787–2795.
doi:10.2514/1.35290
[12] Duffin, D. A., "Feed-Forward Adaptive-Optic Correction of a Weakly-Compressible High-Subsonic Shear Layer," Ph.D. Dissertation, Aerospace and Mechanical Engineering Department, Univ.of Notre Dame, Notre Dame, IN, 2009.
[13] Hugo, R. J., and Jumper, E. J., "Constant Current Anemometry and its Impact on Aero-Optical Measurements," AIAA Paper 1995-1986, June 1995.

M. Visbal
Associate Editor